CORROSION SCIENCE AND TECHNOLOGY, Vol.11, No.3(2012), pp.71~76

Numerical Simulation of Flow and Dross Particle Transfer in a 55% Al-Zn Pot

Hwang Suk Kim†, Jong Gi Kim, Seung Chae Yoon, Hee Joong Im, and Man Been Moon

Hyundai HYSCO Research and Development Center, 313, Donggok-ri, Songsan-myeon, Dangjin-si, Chungnam, Korea
(Received October 31, 2009; Revised June 19, 2012; Accepted June 19, 2012)

Computational fluid dynamics (CFD) is nowadays a powerful and reliable tool for simulating different flow processes and temperature. CFD is used to analyze the various pot geometries and operative variables in 55% Al-Zn pot of CGL. In this research, different strip velocities were assumed and then shown the flow pattern in the pot that was similar in the different strip velocities. Temperature distribution in the pot depended on inductors and inlet strip temperature at the steady condition. Generation of dross particles and transport models were considered to describe dross particles evolution inside the pot. In order to observe dross influence by scrap location, dross particles were generated upon the sink roll. Floating time of dross particles is different by scraper locations above the sink roll.

Keywords *: computational fluid dynamics (CFD), dross particle, Al-Zn pot, flow velocity*

1. Introduction

General and continuous galvanizing in the coating of steel products is used in many cold steel sheet productions.[1)-6)] By far the most important product is hot dip galvanized steel sheet that used for automobile body production. The steel strip is coated by passing it through a pot of molten 55% Al-Zn and withdrawing it from the pot to produce continuous hot dip galvanized steel. It is important for good level and uniformity products to control temperature and aluminum concentrations in the pot. During this process, surface defect by dross occurs when particles of Zn-Fe or Al-Fe stick to the strip surface. This surface defect could be controlled by Al concentration and temperature distribution in the galvanizing pot. The numerical thermo-fluid dynamic model of 55% Al-Zn pot has proven to be a powerful tool to simulate different operative variables and geometrical configurations to understand factors of the surface defects.[7)-9)]

Firstly, the galvanizing pot geometries and process conditions are introduced before the results of the flow pattern and temperature distribution at steady state are presented and discussed.[10)-16)] Finally, the dross distribution and transport in the pot are analyzed at unsteady state. Additionally, particle-tracking simulations were carried by Lagrangian model to trace dross on the sink roll.

2. Geometry and modeling

The galvanizing pot for the CFD is given in Fig. 1. The galvanizing pot has a moving strip, rotating sink roll, correct roll, stabilizer roll and other structures. In this model, four inductors are mounted each side of pot. Each in-

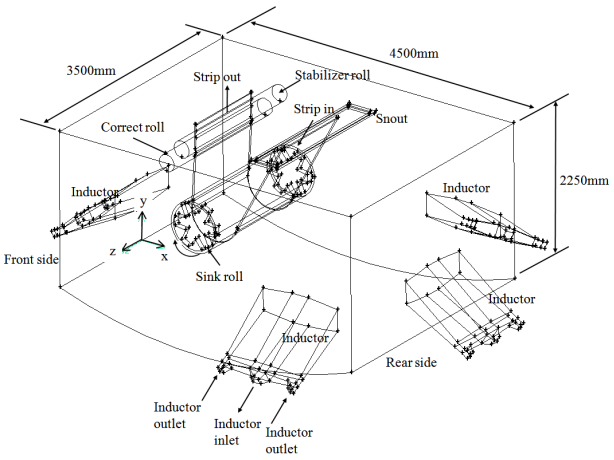

Fig. 1. Geometry model of CGL pot.

† Corresponding author: scyoon@hysco.com

ductor has two outlets at the side and one inlet that are located in the center. The strip enters the zinc pot under an angle of approx. 60° and moving speed are considered 75 mpm and 150 mpm. Sink roll dia. is 800 mm, each dia. of correct and stabilizer roll is 230 mm. Pot dimensions are 4500 mm× 3500 mm× 2250 mm

Fluid dynamic model is incompressible flow of 55% Al-Zn and constant density is considered. Table 1 shows material properties and simulation process boundary conditions. The inductor information for the flow was provided by AJAX which is inductor supplier. The mass, momentum, and energy equations of the flow were solved by FLUENT 6.3. Standard k-ε model is used to solve turbulence.[17)-18)] A Modeling mesh has about 2170000 elements and 400000 nodes.

Fig. 2 illustrates the finite element distribution. For the more accurate flow analysis around the strip and rolls, mesh size around the strip and rolls is smaller than other parts in the pot. Temperature of galvanizing pot is controlled by thermocouple at 600 ℃. Temperature of inlet strip is normally lower than pot; on the other hand input fluid temperature by the inductors is hotter than pot temperature for considering heat balance. A uniform velocity was assumed at the strip line, inlet and outlet inductors. The galvanizing pot surface was assumed to be a free slip wall for numerical calculation. Additionally, ingot dropping in the pot is not considered at the simulation.

Table 1. The material properties and process parameters.

Material	Property	Value	Unit
55%Al-Zn	Density	3327	kg/m^3
	Dyn.viscosity	1.648×10^{-3}	Pa·s
	Spec.heat capacity	860	J/(kg·K)
	Therm. Conductivity	50	W/(m·K)
	Mean temp.	600	℃
Strip	Density	7860	kg/m^3
	Speed	75/150	m/min
	Strip width	1240	mm
	Strip entry temp.	597	℃
Inductor	Specified power	450	kW
	Output metal flow rate	147	MT/Hr
	Quantity	4	EA

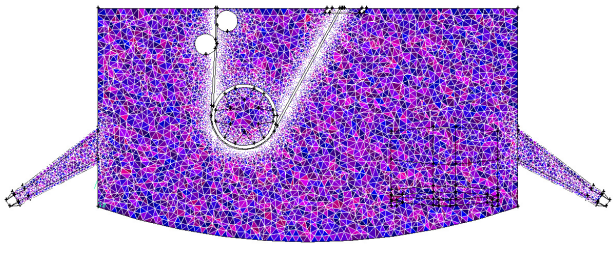

Fig. 2. Finite element distribution of central XY-plane.

3. Fluid dynamic - velocity and temperature field

3.1 Velocity field distribution

The result of flow velocity is given in Fig. 3. The flow velocity is almost equal to strip speed near the moving strip and rolls. High velocity fluid flow fields in the pot are the inductors inlet, outlet, around the sink roll, stabilizer roll and correct roll. Generally, flow moves from the strip entry down to the sink roll and up to the correct roll. Squeeze flow heading to the wall occurs where the strip meets the lower correct roll. This flow is deflected by wall then that is divided into upward flow to the free surface and downward flow to the bottom of pot. Upward flow makes circulating flows below the free surface. Downward flow heads to rear side of the pot along the bottom wall.

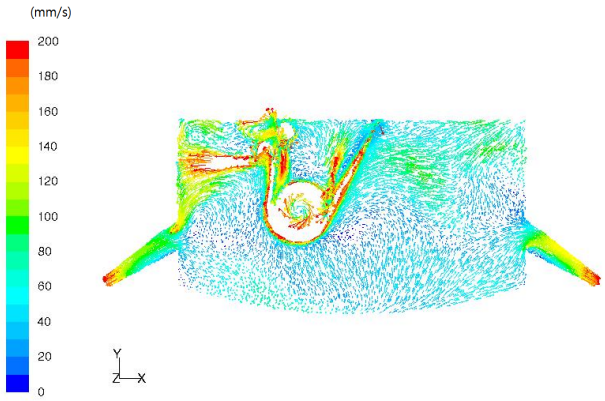

(a) 75 mpm on the strip

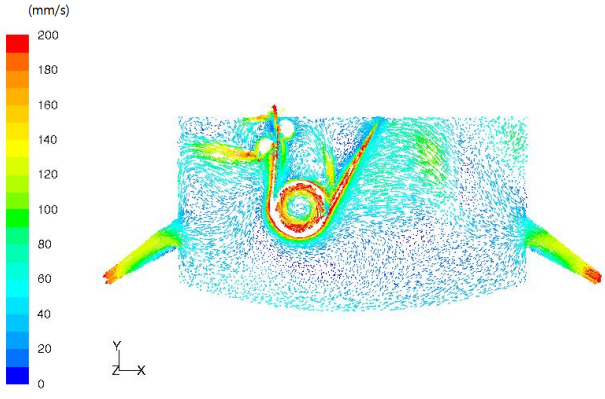

(b) 150 mpm on the strip

Fig. 3. Flow vectors on the central XY- plane.

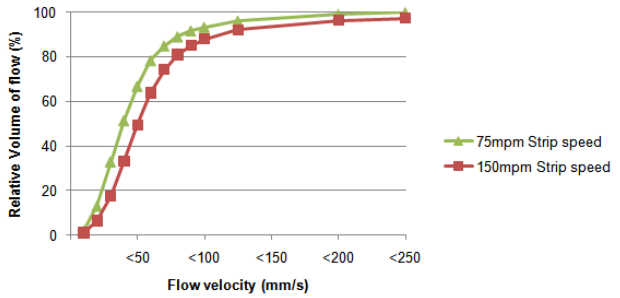

Fig. 4. Relative volume of Flow at 75 mpm and 150 mpm on the strip.

Above the sink roll region that is enclosed by entering and exiting strip, a rapid flow descends with the strip meeting flow moving backwards with the roll surface, so squeeze flow generate toward the free surface. Higher stabilizer-roll and strip movement toward exit makes circulating flows near the free surface. Inside area of the inductor, two recirculation zones are generated between the inductor outlets to inlet.

Fig. 4 shows comparison of relative volume flow of 75 mpm and 150 mpm strip speed. In the 80% of the bath the flow velocity is less than 65 mm/s at 75 mpm and 80 mm/s at 150 mpm strip speed. Therefore the melt 55% Al-Zn velocity of the most regions (80%) in the pot is under 5% of the 75 mpm strip speed and 3% of the 150 mpm strip speed. When strip velocity is higher, dead zones (Fluid velocity is under 10 mm/s) are decrease. Additionally Simulation results show that flow pattern is similar none the less because strip speed is different.

3.2 Temperature field distribution

Galvanizing pot has 4 inductors which located each side of walls. Every walls and the free surface are isothermal condition, so inductors input the heated liquid Zinc into the pot to maintain the temperature at the constant condition. CFD analysis does not consider heat loss on the walls and free surface but heat flux at inductor

Fig. 5, 6 shows the temperature distribution by the strip speed. The central XY-plane and top view of both cases are shown that the highest temperatures are observed rear region of the pot. There are 3 inductors mounted on the side walls. Also, the results predict that inside the strip has low temperature region in the pot. Low temperature region consist two kinds of factors. One is that the Strip obstructs the hotter flow from inductors to inside the strip region. The other is that entry temperature of the strip is lower than pot temperature. Bottom of the pot is lower temperature which is caused by hotter metal flowing to diagonal upwards from outlet inductors on the side walls. At the exit of the strip, the inductor outlet flow is prevented from rising flow along the strip movement to the free surface. For 75 mpm strip speed, the average pot temperature is 600 ℃ and deviation is ± 5 ℃. 150mpm strip speed has less temperature variation than 75 mpm. 150 mpm strip speed have higher flow rate in the same boundary conditions and enables more uniformed temperature distribution in the pot.

4. Dross distribution

4.1 Dross distribution in the pot

In order to get more information about the influence by the strip speed, dross particle simulations were carried out by the strip speeds. Table 2 (a) shows dross properties of the simulation. The initial uniform distribution of dross is considered 1.5% volume and 0.1 mm diameter particles in the pot. Particle transport is used Eulerian model for continuous particle concentration. Fig. 7 shows dross distribution by volume fraction in 75 mpm and 150 mpm strip speed. For the 0.1mm diameter particles, bottom region is higher volume fraction than upper region in the

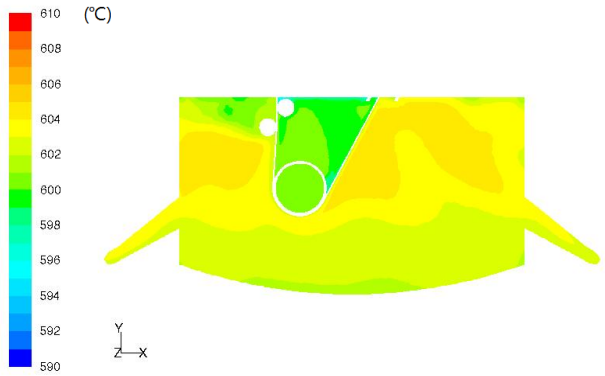

(a) 75 mpm on the strip

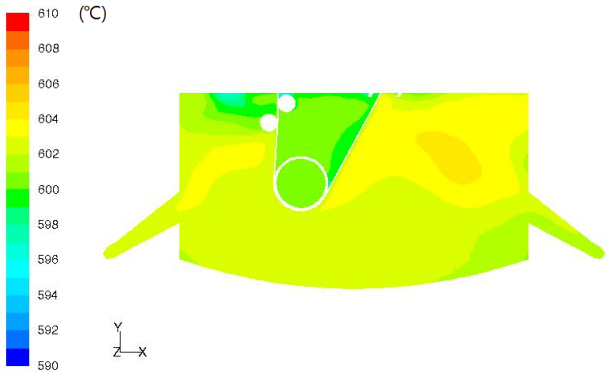

(b) 150 mpm on the strip

Fig. 5. Temperature distribution on the central XY- plane.

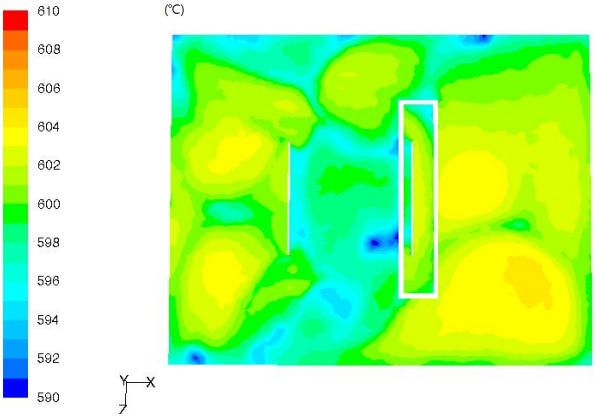

(a) 75 mpm on the strip

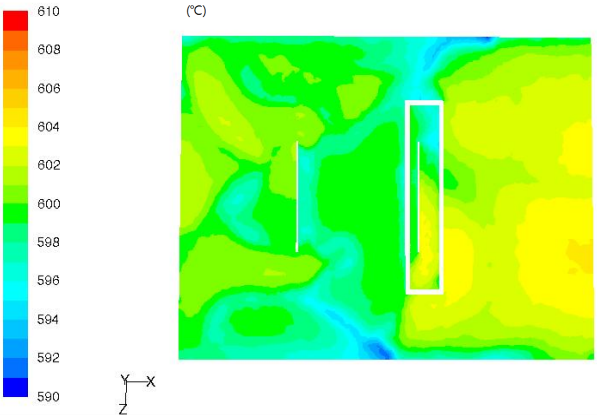

(b) 150 mpm on the strip

Fig. 6. Temperature distribution on the top view.

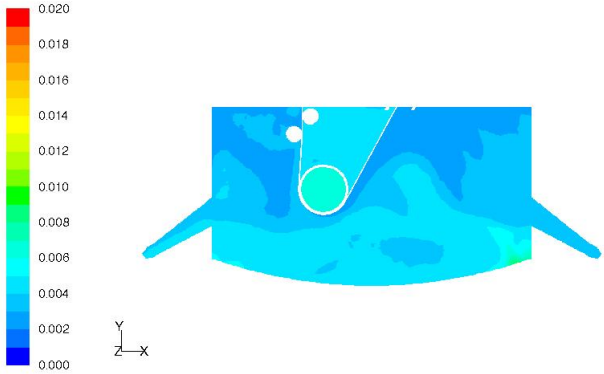

(a) 75 mpm on the strip

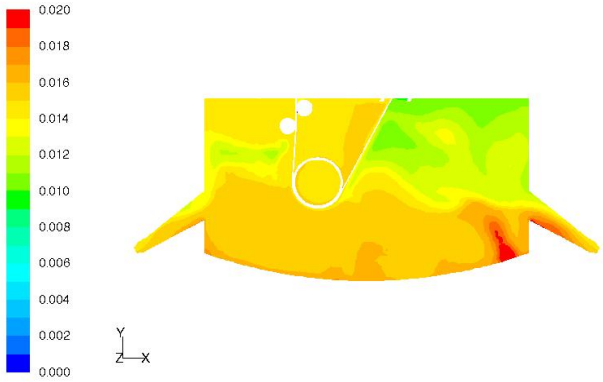

(b) 150 mpm on the strip

Fig. 7. Dross volume fraction by Eulerian model.

Table 2. Process parameters

(a) Material properties of dross

Material	Property	Value	Unit
Dross	Density	3426	kg/m^3
	Diameter	0.1	mm

(b) Process parameters for dross particle trace

Case	Dross location	Strip speed (m/min)
1	-20°	75
2	-20°	150
3	+38°	75
4	+38°	150

pot. In the results of both cases, the bottom region of rear side is settled by the number of particles over time. In the case of 150 mpm strip speed, the proportion of particles settling at the bottom on the pot is higher than 75 mpm.

4.2 Dross particle flow pattern upon the sink roll

In order to get more insight about surface defect on the strip by dross, particle-tracking simulations were carried. Table 2 (b) shows process parameters for the dross particle trace. Dross generated positions are considered two cases by scrap position on the sink roll. Fig. 8 shows dross generation position in case 1, 2 and 3, 4. To compare influence of the positions where dross particles generated, transport model is considered the Lagrangian model. The complex flow pattern of the dross and the independent particle movement are solved by Lagrangian model. Particle size of dross is 0.1mm and density is around 3420 kg/m^3 at 600 ℃. Strip speed is considered 75 mpm on the strip and 150 mpm on the strip. The Particles are able to lose energy when particles collide with the pot wall.

As the results in Fig. 9, near the entry position of the strip has less dross floating time in the pot than exit position above the sink roll. 75 mpm and 150 mpm on the strip have similar dross pattern in the pot. However, when strip moving velocity is 150 mpm, the dross goes down to the bottom more quickly than 75 mpm. The above ob-

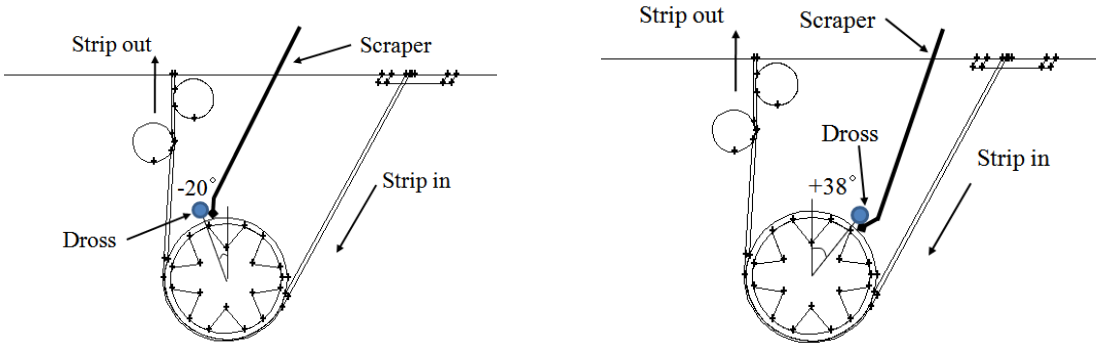

(a) case 1, case 2 (b) case 3, case 4

Fig. 8. Initial location of dross particles above the sink roll.

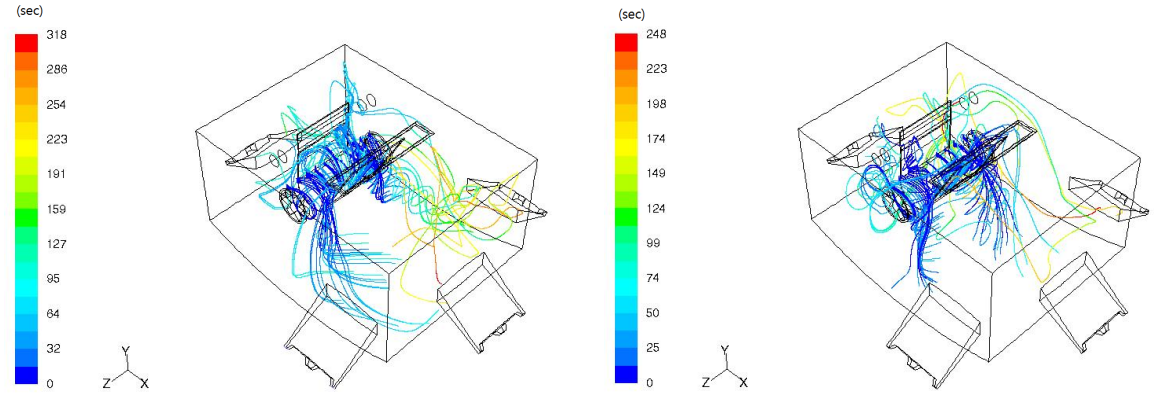

(a) Case 1 (Average time - 105 sec) (b) Case 2 (Average time - 63 sec)

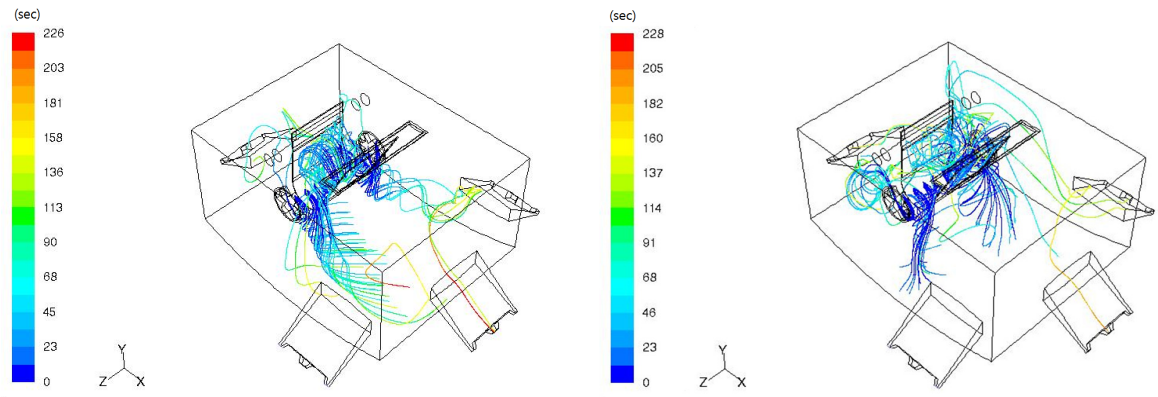

(c) Case 3 (Average time - 87 sec) (d) Case 4 (Average time - 59 sec)

Fig. 9. Dross streamlines above the sink roll.

servations support that the 150 mpm strip speed and entering strip position have less dross floating time in the pot then 75 mpm.

5. Conclusions

3D CFD simulations have been used to solve the flow patterns, temperature and dross distributions in the zinc pot. Strip speed is considered 75 mpm and 150 mpm. The fluid flows are similar pattern both velocities. High velocity areas are limited to the surround of strip, rolls and inductors. Flow velocities of 80% regions in the pot are under 65 mm/s at 75 mpm and 80 mm/s at 150 mpm strip speed. Therefore, 150 mpm strip speed has faster ve-

locity distribution in the pot than that of 75 mpm strip speed.

High temperature regions are near the inductors and rear upper area in the pot. Low temperature region is inside the strip above the sink roll. This is cause of two factors. One is that strip obstruct the hotter flows from inductors. The other is that entry temperature of the strip is lower than pot temperature. In case of 150 mpm strip velocity has higher flow rate at same conditions, and it makes more uniformed temperature distribution in the pot. Therefore, 150 mpm strip speed has less temperature variation than 75 mpm.

Eulerian model is considered for time dependent to solve dross distribution. The bottom region is settled by the number of particles over time. In order to get more insight about surface defect on the strip by dross, particle-tracking simulations were carried. Dross is generated when sink roll is scrapped in the pot. Simulations considered four cases by scrap position and strip speed and Lagrangian model is considered to observe particle trace above the sink roll. Case 3, 4 positions where are scrapping position near the entering strip on the sink roll has less dross floating time than case 1, 2 position where is near the exit strip at same strip velocity. Additionally, 150 mpm strip velocity has less time to sink down dross to the bottom than 75 mpm. It draws an inference that 150 mpm strip velocity and the area around strip entry have less dross floating time in the pot.

References

1. A. Nasser, A. Yadav, P. Pathak, and T. Altan, *J. Mater. Proc. Tech*., **210**, 429 (2010).
2. I. Mejia, A. Bedolla-Jacuinde, C. Maldonado, and J. M. Cabrera, *Mater. Sci. Eng. A*, **528**, 4468 (2011).
3. C. Nikhare, P. D. Hodgson, and M. Weiss, *Mater. Sci. Eng. A*, **528**, 3010 (2011).
4. T. Uemori, T. Okada, and F. Yoshida, *Key Eng. Mater*., **177**, 497 (2000).
5. D. W. Leu, *J. Mater. Proc. Tech*., **66**, 9 (1997).
6. R. M. Cleveland and A. K. Ghosh, *Inter. J. Plasticity*, **18**, 769 (2002).
7. J. B. Kim and S. K. Lee, *Corros. Sci. Tech*., **26**, 191 (1997).
8. J. B. Kim and S. K. Lee, *Corros. Sci. Tech*., **30**, 247 (2001).
9. D. Phelan, *Galvatech*, **6**, 961, (2004).
10. C. H. Ellen and C. V. Tu, *J. Fluids Eng*., **106**, 399 (1984).
11. Y. H. Kim, Y. W. Cho, S. H. Chung, J. D. Shim, and H. Y. Ra, *ISIJ*, **44**, 369 (2005).
12. Y. H. Kim, Y. W. Cho, S. H. Chung, J. D. Shim, and H. Y. Ra, *ISIJ*, **40**, 706 (2000).
13. S. J. Lee, S.Kim, M. S. Koh, and J.H. Choi, *ISIJ*, **42**, 407 (2002).
14. F. Bezzo, S. Macchietto, and C. C. Pantelides, *Com. Chem. Eng*., **28**, 501 (2004).
15. M. A. Hoef, M. S. Annaland, and J. A. M Kuipers, *Chem. Eng. Sci*., **59**, 5157 (2004).
16. Y. Takeishi and H. Morino, *ISIJ*, **40**, 1127 (2000).
17. K. C. Ro and H. S. Ryou, *J. Com. Fluids. Eng*., **15**, 1 (2010).
18. N. G. Wright and G. J. Easom, *Appl. Math. Model*., **27**, 1013 (2003).